Liquid-phase reactions of aromatic organosulfates with OH radicals: Kinetics, mechanisms, and environmental effects

Yu Yang[1], Caiqing Yan[1], Ruyu Yuan[1], Ping Liu[1], Hanyuan Zhang[1], Haibiao Chen[1], Yujiao Zhu[1], Hengqing Shen[1], Yan Wu[2], Likun Xue[1] and Liubin Huang[1*]

[1]Environment Research Institute, Shandong University, Qingdao, Shandong 266237, China
[2]School of Environmental Science and Engineering, Shandong University, Qingdao, Shandong 266237, China

Correspondence to: Liubin Huang (hliubin@sdu.edu.cn)

Abstract. Aromatic organosulfates (aromatic OSs) are widely detected in the atmosphere and exhibit high abundance in urban areas. However, the atmospheric fate and environmental impacts of aromatic OSs remain poorly understood. In this study, we investigated the liquid-phase reactions of three aromatic OSs (i.e., phenyl sulfate, p-tolyl sulfate, and 4-ethylphenyl sulfate) with OH radicals (•OH). The second-order reaction rate constants (k) of aromatic OSs with •OH were measured in the range of 4.3–6.4×10^9 M^{-1} s^{-1} at different pHs. It is found that k values are similar for the homologues of aromatic OSs, whereas they are slightly affected by the solution pHs. These three aromatic OSs oxidized by •OH mainly yielded functionalized OSs, along with fragmented OSs and inorganic sulfate. The observation of inorganic sulfate formation, for the first time, indicates that aromatic OSs can also be converted into inorganic sulfate in analogous to aliphatic OSs. Furthermore, generated functionalized OSs can significantly enhance the light absorption capacity, particularly under acidic conditions. These findings provide new insights into the understanding of the fate of aromatic OSs in the atmosphere that they can rapidly undergo atmospheric transformation, affecting the atmospheric sulfur cycle and altering aerosol optical properties.

1 Introduction

Secondary organic aerosols (SOA) play a significant role in regional air quality, climate change, and public health (Shrivastava et al., 2017; Peng et al., 2023; Liu et al., 2022). Organosulfates (OSs), organic compounds characterized by a sulfate ester functional group (R–O–SO_3^-), have been widely detected in SOA in various environments (from remote to highly polluted) (Kristensen et al., 2011; Zhang et al., 2012; Hansen et al., 2014; Hu et al., 2015; Wang et al., 2018; Ma et al., 2025), accounting for up to 30% of particulate organic mass (Surratt et al., 2008; Lukács et al., 2009; Tolocka and Turpin, 2012; Li et al., 2025). OSs can be produced from the reactions involving either biogenic volatile organic compounds (VOCs) such as isoprene and monoterpenes, or anthropogenic VOCs such as diesel fuel vapor and aromatics (Hettiyadura et al., 2019; He et al., 2022; Wang et al., 2022; Thomas et al., 2025). In remote or clean areas, OSs were typically measured with the structure characterization of isoprene, monoterpenes, and their derivatives (Surratt et al., 2008; Zhang et al., 2012; Hettiyadura et al., 2017). For example, Thomas et al. (2025) reported that IEPOX-OS ($C_5H_{12}O_7S$) is the dominant species of OSs in aerosols in the Amazonian rainforest. In urban areas, in addition to isoprene and monoterpenes derived OSs, other OSs containing an aromatic ring were

also observed in collected aerosols (Kundu et al., 2013; Huang et al., 2018; Wang et al., 2021; He et al., 2022). He et al. (2022) identified four kinds of aromatic OSs (i.e., phenyl sulfate, methylphenyl sulfate, benzyl sulfate, and phenethyl sulfate) with concentrations ranging from 0.04 ± 0.08 to 2.37 ± 3.59 ng m^{-3} in $PM_{2.5}$ collected in Chengdu, China. Previous study observed that aromatic OSs can account for up to 63.5% of the total identified OSs in a megacity in China (Ma et al., 2014).

Extensive research has been conducted to elucidate the mechanisms of OS formation in the atmosphere. The proposed formation mechanisms include: (a) the reactive uptake of epoxides on acidic sulfate aerosols. This pathway has been established as an important mechanism for the formation of isoprene-derived OSs (Surratt et al., 2010; Lin et al., 2013; Riva et al., 2019; Lei et al., 2022); (b) the multiphase reactions of unsaturated hydrocarbons with either sulfate radical ($\bullet SO_4^-$) or sulfur dioxide (SO_2). Previous studies revealed that the addition of $\bullet SO_4^-$ on the C=C bond can result in the formation of OSs in aqueous aerosols (Nozière et al., 2010; Schindelka et al., 2013), and SO_2 can effectively react with unsaturated fatty acids to form OSs (Shang et al. 2016; Passananti et al. 2016); (c) heterogeneous reactions of organic peroxides with SO_2. Recent laboratory studies have shown that SO_2 can also be oxidized by organic peroxides rapidly with the production of OSs other than sulfate (Wang et al., 2019; Yao et al., 2019, 2023); (d) substitution reaction of organic nitrates (ONs) by sulfate (Darer et al., 2011; Hu et al., 2011). Darer et al. (2011) and Hu et al. (2011) observed the formation of OSs during the processes of ON hydrolysis in the presence of H_2SO_4; (e) acid-catalyzed esterification of alcohols. While laboratory studies reported OS formation from sulfate esterification (Iinuma et al., 2007), subsequent kinetic studies suggested that this reaction is too slow under typical tropospheric conditions (Minerath et al., 2008).

Compared to the formation of OSs, understanding of the fate of OSs is still limited. Hydrolysis has been identified as an atmospheric removal process for certain OSs, with rates depending on the acidity of the aerosol and the molecular structure (Darer et al., 2011; Hu et al., 2011; Mael et al., 2015). Tertiary OSs were found to hydrolyze effectively under acidic conditions, while primary and secondary OSs were relatively stable. Additionally, OSs can also be further oxidized by OH radicals (•OH) after formation. Lai et al. (2024) investigated the kinetics of reactions of methyl sulfate and ethyl sulfate with •OH, finding that the rate constant (k) may be significantly affected by the carbon chain length. This finding was also confirmed for more kinds of aliphatic OSs (i.e., methyl sulfate, ethyl sulfate, and propyl sulfate) (Gweme and Styler, 2024). Chen et al. (2020b) detected the products of 2-methyltetrol sulfate diastereomers (IEPOX-OS) oxidized by •OH heterogeneously, observing various fragmented and functionalized OSs after reactions, which their formation pathways were previously unknown in the atmosphere. During the oxidation of some OSs (e.g., methyl sulfate, ethyl sulfate, 2-methyltetrol sulfate, and α-pinene derived OSs) by •OH, it is interesting to find that OSs can also return to inorganic sulfate except for new OS formation (Kwong et al., 2018; Xu et al., 2020, 2024). In addition to laboratory studies, Tsona et al. (2025) employed quantum chemical calculation based on density functional theory to verify the formation of inorganic sulfate from the gas-phase and aqueous-phase reactions of OSs with •OH. It should be noted that the currently limited research about the fate of OSs has focused on the biogenic OSs or small alkyl OSs, little is known about the kinetic and mechanism for the conversion of aromatic OSs, which is another important kind of OSs, particularly in the urban aerosols. A very recent study investigated the liquid-phase •OH oxidation of phenyl sulfate other than aliphatic OSs (Gweme and Styler, 2024), observing that the k value of phenyl sulfate is much faster

than that of aliphatic OSs. After reactions, they observed the new OSs formed (e.g., hydroxyphenyl sulfate and dihydroxyphenyl sulfate), but without any evidence of inorganic sulfate production. However, whether aromatic OSs can be converted into inorganic sulfate or not remains unclear since they did not observe the presence of inorganic sulfate for aliphatic OSs as well. Therefore, to better characterize and understand the liquid-phase reactions of aromatic OSs with •OH, further research is warranted.

In this study, we investigated the liquid-phase reactions of atmospherically relevant aromatic OSs (i.e., phenyl sulfate, p-tolyl sulfate, and 4-ethylphenyl sulfate) with •OH. Our study aims to explore the influence of substituent structure on reaction kinetics and elucidate the mechanisms for the conversion pathways of aromatic OSs in the atmosphere. Moreover, given that the oxidation of aromatic organic compounds often induces significant alteration in the optical properties of the reaction system (Li et al., 2021; Arciva et al., 2024), the changes in optical properties were also examined.

2 Materials and methods

2.1 Batch reactor experiments

Experiments of the liquid-phase •OH oxidation of aromatic OSs were carried out in a 150 mL custom-built quartz reactor thermostated by a water jacket. OH radicals were generated through the aqueous photolysis of 10 mM H_2O_2 (30%, Hu Shi) under irradiation from a 300 W Xenon arc lamp to simulate sunlight. Three commercial aromatic OSs (i.e., phenyl sulfate (≥98%, Macklin), p-tolyl sulfate (≥98%, Macklin), and 4-ethylphenyl sulfate (≥98%, Sigma-Aldrich) used as representative of aromatic OSs. The solution containing each aromatic OS, H_2O_2, and dissolved O_2 was introduced into the quartz reactor with a total volume of 100 mL, and was agitated by an electromagnetic stirrer. Subsequently, the reactor was sealed, and the lamp was ignited to start the reaction. Given the varied pH values in aqueous environments in the atmosphere (from 1 to 9) (Herrmann et al., 2015; Pye et al., 2020), the solution was adjusted to pH 3 (using 36–38% HCl, Hu Shi) and pH 8 (using phosphate buffer (Na_2HPO_4 and NaH_2PO_4)) to represent acidic and alkaline conditions, respectively. All experiments were performed at 298 K at least in duplicate. Details about the information of the experiments carried out in this study are summarized in Table S1.

Kinetic experiments were performed with 0.05 mM of each aromatic OS in the presence of a reference compound (i.e., sodium benzoate (BA, 98%, Macklin)) over the reaction time of 2 hours. Two sets of control experiments were carried out. One involved irradiating a solution of each aromatic OS alone to investigate the effects of light only. Another set combined each aromatic OS with H_2O_2 in the dark to preclude the interference from H_2O_2. Reaction progress was tracked by withdrawing 1 mL aliquots at 30-minute intervals for direct analysis via either ultrahigh-performance liquid chromatography (UPLC, Agilent 1260) or ion chromatography (IC, Dionex ICS-600), without any intermediate processes or dilution. Mechanism experiments were conducted the same as the kinetic experiments, except that BA was not added. After reactions, 0.5 mL of the sample was taken and was immediately stored at –20 °C prior to product analysis using ultra-performance liquid chromatography equipped with a quadrupole time-of-flight mass spectrometer (UPLC-Q-TOF-MS, Bruker Impact HD). Control experiments of each

aromatic OS and H_2O_2 in the dark were also performed for comparison in order to eliminate the possibility of detected products resulting from analytical artifacts. To enhance the detection of optical changes, we also conducted experiments at higher aromatic OS concentrations (0.5 or 1 mM) over an extended period of 8 hours. For these experiments, the sample was taken every 4 hours for immediate measurement of its absorbance spectra using a UV–vis spectrophotometer (Duetta™, Horiba Scientific) and excitation–emission matrix (EEM) fluorescence spectra by a fluorescence spectrometer (Duetta™, Horiba Scientific). After reactions, the sample was also analyzed by ultrahigh-performance liquid chromatograph coupled with a photodiode array detector and an Orbitrap mass spectrometer (UPLC-PAD-MS, Thermo Fisher Scientific) to investigate how optical changes were affected by the formation of chromophores. 0.5 mL sample was diluted with 0.5 mL H_2O and 0.25 mL acetonitrile, and then the resulting solution was stored at –20 ℃ before analysis.

2.2 Kinetic measurements

The second-order rate constant of each aromatic OS with •OH was measured by the competition kinetic method using 0.05 mM sodium benzoate as the reference compound (Smith et al., 2015). It is noted that one of the important principles of this method is that aromatic OS and the reference compound are consumed only by •OH oxidation in the liquid phase. Control experiments of the direct photolysis of each aromatic OS without the addition of H_2O_2 as well as the reactions of each aromatic OS, BA, and 10 mM H_2O_2 without illumination were carried out to preclude interferences from other reactions. Figures S1 and S2 show that the influences of either hydrolysis or photodegradation on the kinetic measurements of these three aromatic OSs are negligible, verifying that the decay of reactants results from •OH oxidation. Therefore, in this study, the second-order rate constant for aromatic OS (k_{OS}) can be calculated using the equation (E1) based on the following reactions (R1 and R2).

$$\ln\left(\frac{[OS]_0}{[OS]_t}\right) = \frac{k_{OS}}{k_{ref}} \ln\left(\frac{[ref]_0}{[ref]_t}\right) \quad \text{(E1)}$$

$$\text{Aromatic OS} + \bullet\text{OH} \rightarrow \text{Products}, k_{OS} \quad \text{(R1)}$$

$$\text{Reference} + \bullet\text{OH} \rightarrow \text{Products}, k_{ref} \quad \text{(R2)}$$

Where [OS] and [ref] are concentrations of aromatic OS and the reference compound (BA) (time =0 and t). The time dependence of aromatic OS consumption is shown in Fig. S3. k_{ref} is the rate constant of BA with •OH. k_{ref} value at pH 3 and 8 was reported as $4.3 \pm 0.8 \times 10^9$ M^{-1} s^{-1} and $6.3 \pm 0.2 \times 10^9$ M^{-1} s^{-1}, respectively (Buxton et al., 1988). Figure 1 displays the relative kinetic plots for aromatic OSs oxidized by •OH under acidic (pH 3) and basic (pH 8) conditions. These plots exhibit strong linearity ($R^2 \geq 0.99$), with the slope of each linear fit corresponding to the k_{OS}/k_{ref}. According to the slope and value of k_{ref}, the k_{OS} can be calculated.

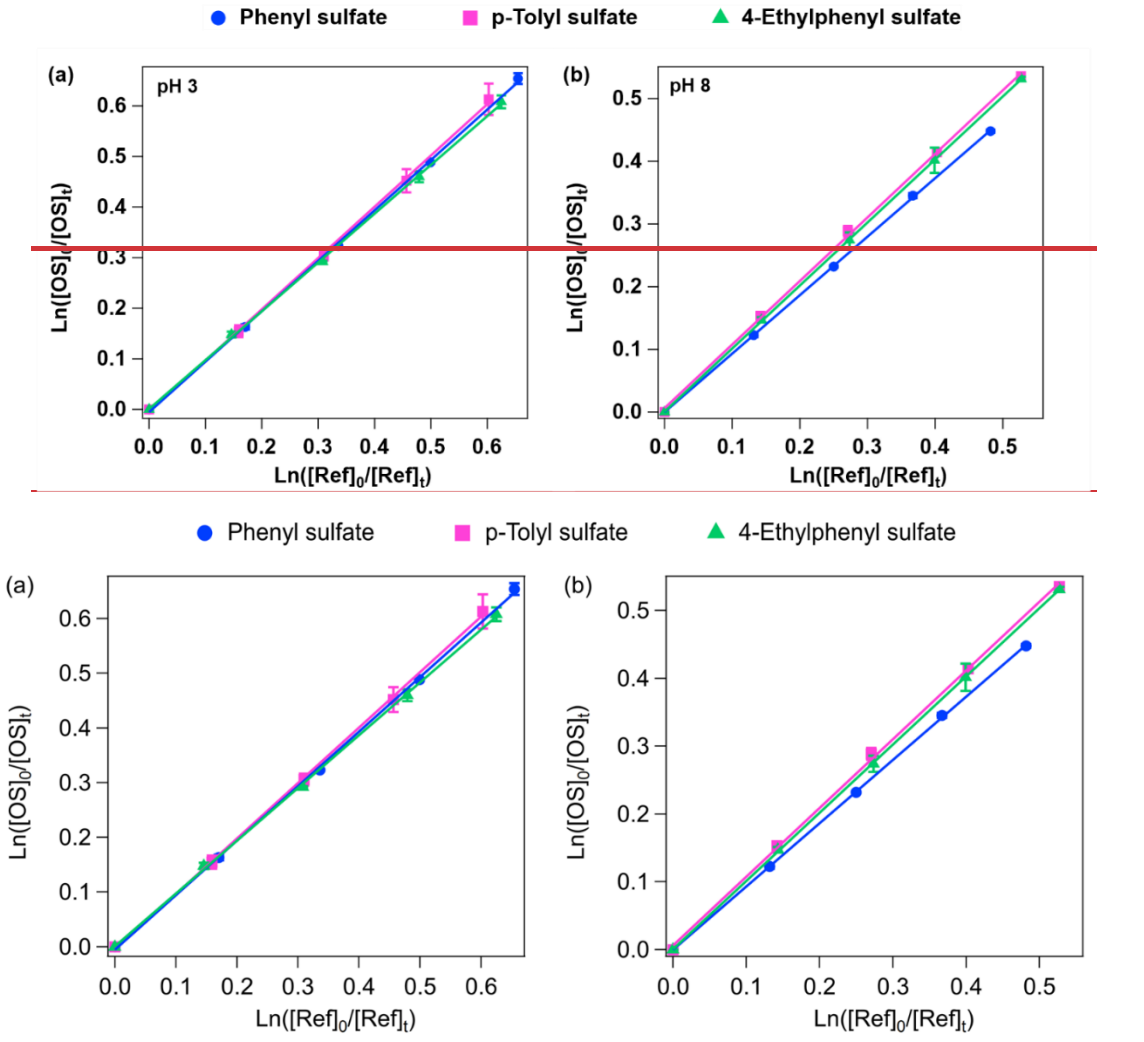

Figure 1. Loss of aromatic OSs and BA during the process of the liquid-phase •OH oxidation at (a) pH 3 and (b) pH 8.

2.3 Reactant and product analysis

The concentrations of aromatic OSs and BA were detected using a UPLC coupled with a UV detector operating at 254 nm. Chromatographic separation was performed on a ZORBAX Eclipse Plus C18 column (4.6 mm × 250 mm, 5 μm) maintained at 40 °C. The mobile phase consisted of acetonitrile and 0.1% formic acid aqueous solution (20:80, v/v) delivered at a flow rate of 0.8 mL min^{-1}, with an injection volume of 10 μL. Quantification of aromatic OSs and BA was achieved by calibration curves (Fig. S4) based on their corresponding peak areas in the chromatogram.

Inorganic sulfate was analyzed by IC with an analytical column (AS 11-HC, 4 × 250 mm, IonPac) and a guard column (AG11-HC, 4 mm × 250 mm, IonPac). The eluent was 20 mM potassium hydroxide at a flow rate of 1 mL min^{-1}.

Reaction products were detected using a UPLC-Q-TOF-MS. Separation was achieved on a C18 column (4.6 mm × 250 mm, particle size = 5 μm; ZORBAX Eclipse Plus) at 40 ℃, with a mobile phase of pure water and acetonitrile (40:60, v/v) at a flow rate of 1 mL min^{-1}. The mass spectrometer was equipped with an electrospray ionization (ESI) source operated in the negative (-) ionization mode. The instrumental conditions for the (-) ESI-MS analysis were as follows: capillary voltage, 4000 V; gas temperature, 200 ℃; dry gas flow rate, 5 L min^{-1}; and nebulizer pressure, 0.4 bar. Data were collected over the mass range of 50–500 Da. We also conducted complementary chromophore product analyses using a UPLC-PAD-MS. Separation was carried out on a C18 column (4.6 mm × 250 mm, particle size = 5 μm; ZORBAX Eclipse Plus) at 40 ℃, with a binary mobile phase consisting of acetonitrile and 0.1% formic acid (20:80, v/v) delivered at a flow rate of 0.8 mL min^{-1}. Mass spectrometric detection was conducted in negative ionization mode over a mass range of 50–500 Da, with the spray voltage set at –3.0 kV, the capillary temperature at 320 °C, the S-lens RF level at -50 V, the sheath gas (nitrogen) pressure at 2.76×10^5 Pa, and the auxiliary gas (nitrogen) flow rate at 3.33 L min^{-1}.

2.4 UV-vis absorption and fluorescent spectra

The light absorption spectra of samples during the processes of reactions were collected using a UV–vis spectrophotometer with a scanning interval of 1 nm in the range of 250–700 nm. A reference absorption spectrum of hydrochloric acid solution (pH 3) or phosphate buffer solution (pH 8) was recorded in the same cuvette before sample analysis for baseline correction. The excitation-emission matrix (EEM) fluorescence spectra were recorded by a fluorescence spectrometer. The excitation wavelength (Ex) and emission wavelength (Em) of EEM were both set to the range of 250–600 nm. The scanning intervals were set to 5 nm and 2 nm. Hydrochloric acid solution (pH 3) or phosphate buffer solution (pH 8) was used as a blank to correct the data as well.

3 Results and discussion

3.1 Kinetics of liquid-phase reaction of aromatic OSs with •OH

The k_{OS} values of three aromatic OSs (i.e., phenyl sulfate, p-tolyl sulfate, and 4-ethylphenyl sulfate) reacted with •OH are summarized in Table 1. At pH 3, the k_{OS} value of phenyl sulfate was measured as $4.3 \pm 0.1 \times 10^9$ M^{-1} s^{-1}. This value is comparable to the literature result of phenyl sulfate at pH 2 using pimelic acid as the reference compound ($5.34 \pm 0.06 \times 10^9$ M^{-1} s^{-1}) (Gweme and Styler, 2024). The slight difference may be attributed to the reference compound selection and the experimental conditions. Values of k_{OS} for the other two aromatic OSs were similar to that of phenyl sulfate (Table 1). The similar k_{OS} value among these three aromatic OSs suggests that the substituent carbon chain length on the aromatic ring has a negligible effect on the reaction kinetics. This observation is quite different from that for alkyl OSs, which shows that k_{OS} is strongly dependent on the carbon number of OS molecule contained (Lai et al., 2024; Gweme and Styler, 2024). Lai et al. (2024) reported that k_{OS} of ethyl sulfate ($3.8 \pm 0.1 \times 10^8$ M^{-1} s^{-1}) was approximately five times higher than that of methyl sulfate ($7.5 \pm 0.1 \times 10^7$ M^{-1} s^{-1}). Gweme and Styler (2024) also found that k_{OS} value increased with increasing carbon chain

length for methyl sulfate ($1.03 \pm 0.21 \times 10^8$ M^{-1} s^{-1}), ethyl sulfate ($4.07 \pm 0.17 \times 10^8$ M^{-1} s^{-1}), and propyl sulfate ($1.22 \pm 0.03 \times 10^9$ M^{-1} s^{-1}). This distinct behaviour may be ascribed to the different mechanisms for aromatic OSs and alkyl OSs oxidized by •OH. For aromatic OSs, the OH radical predominantly attacks the aromatic ring with multiple addition sites (Bloss et al., 2005; Garmash et al. 2020). While alkyl OSs react primarily through hydrogen abstraction, the increasing carbon chain length can enhance reactivity through the inductive effect of $-CH_x$ groups, the increasing electron density at the hydrogen abstraction site, and the stabilization of resulting alkyl radicals (Dorfman and Adams, 1973; Monod and Doussin, 2008). As such, aromatic OSs have higher reactivity compared to alkyl OSs. The negligible effect of carbon number on the reactivity of aromatic compounds was also observed in other homologues of aromatic compounds. For example, Schuler and Albarran (2002) reported a similar rate constant for the reactions of toluene (8.1×10^9 M^{-1} s^{-1}) and benzene (7.8×10^9 M^{-1} s^{-1}) with •OH. It is noted that the k_{OS} values are lower than those of their parent aromatic hydrocarbons. This reduction in reactivity may be attributed to the electron-withdrawing effect of the $-OSO_3^-$ groups, which can reduce the reactivity of the aromatic ring toward •OH (Lai et al., 2024).

Table 1. The second-order rate constant (*k*) of aromatic OSs reacting with •OH in the liquid phase at different pHs.

Species	*k* (10^9 M^{-1} s^{-1})	
	pH = 3	pH = 8
Phenyl sulfate	4.3 ± 0.1	5.9 ± 0.1
p-Tolyl sulfate	4.4 ± 0.1	6.4 ± 0.2
4-Ethylphenyl sulfate	4.5 ± 0.1	6.3 ± 0.1
Benzoic acid[a]	4.3 ± 0.8	6.3 ± 0.2

[a] Rate constants for benzoic acid are obtained from Buxton et al. (1988).

Table 1 shows that the carbon chain length has an insignificant effect on the k_{OS} values of aromatic OSs at pH 8 as well. k_{OS} values of phenyl sulfate, p-tolyl sulfate, and 4-ethylphenyl sulfate were calculated as $5.9 \pm 0.1 \times 10^9$, $6.4 \pm 0.2 \times 10^9$, and $6.3 \pm 0.1 \times 10^9$ M^{-1} s^{-1} at pH 8, respectively. These values were higher than those measured at pH 3. It should be noted that different matrices (HCl *vs* phosphate buffer) were used to adjust the solution pH, and the ionic strength of the solution is different at different pHs. The ionic strength of solution at pH 3 and pH 8 was estimated as 1×10^{-3} M and 6.9×10^{-3} M, respectively. Previous study reported that a substantial increase in ionic strength from ca. zero to 6.5 M only resulted in a tenfold decrease in k_{OS} value of phenyl sulfate (Gweme and Styler, 2024). Therefore, the relatively low ionic strength variation between pH conditions in this study may not account for the observed differences in k_{OS} values of aromatic OSs. Gweme and Styler (2024) measured the k_{OS} of phenyl sulfate at pH 2 and pH 9, observing that it is pH independence. They attributed this pH independence to phenyl sulfate remaining fully deprotonated (pKa = –2.2) across the entire experimental pH range. However, previous studies demonstrated that even though methoxyphenol, benzene-diols, and highly substituted phenol mainly exist in their protonated form within the pH range of 2–6, their *k* values at pH 2 were generally lower than those at pH 5 or 6 (Arciva et al., 2022). One possible explanation is that the acidic condition could hinder •OH attack on aromatic systems or reduce the lifetime of hydroxycyclohexadienyl radical intermediates, slowing irreversible diol formation (Smith et al., 2015).

Another possible explanation is the uncertainty of the *k* of the reaction of reference compound with •OH (Arciva et al., 2022). Therefore, the difference and uncertainty of the rate constant of the reference compounds selected may also explain the discrepancy between the findings of Gweme and Styler (2024) and our study.

3.2 Product measurements and reaction mechanism

In this study, products generated from the liquid-phase reactions of three aromatic OSs with •OH were characterized by mass spectrometry. The identified species were consistent across both pH 3 and pH 8 conditions. The observation that product intensities were substantially higher under illumination conditions than in dark controls implies that these products arise from •OH oxidation, not from analytical artifacts or hydrolysis (Fig. S5). Table S2 lists the identified products from the reaction of phenyl sulfate with •OH. The predominant signals corresponded to hydroxyphenyl sulfate ($C_6H_5O_5S^-$, *m/z* 189) and dihydroxyphenyl sulfate ($C_6H_5O_6S^-$, *m/z* 205), aligning with previous work (Gweme and Styler, 2024). Additionally, the multiple –OH group addition products (e.g., $C_6H_5O_7S^-$) were also detected. As illustrated in Fig. 2, •OH-initiated oxidation of phenyl sulfate follows a mechanism analogous to conventional aromatic compounds (e.g., benzene). The reaction initiates via the addition of •OH to the aromatic ring, generating hydroxycyclohexadienyl radicals (OH-PS radicals) (Lay et al., 1966; Minakata et al., 2015). OH-PS radicals rapidly react with O_2 to yield phenolic compounds that can undergo further multi-step •OH additions to form these polyhydroxy products ($C_6H_5O_nS^-$, n=5–7). Alternatively, OH-PS radicals can also react with O_2 to form peroxyl radicals (RO_2•). The reversible cyclization of RO_2• and the subsequent O_2 addition generate bicyclic RO_2•. Bicyclic RO_2• can react with RO_2• to produce ring-opening products as shown in Table S2 (Wang et al., 2013; Dong et al., 2021). Fragmented OS formation resulting from ring-opening pathways during •OH oxidation of aromatic OSs has not been reported previously. Notably, some of these ring-opening fragments (e.g., $C_2H_3O_5S^-$, $C_5H_7O_8S^-$) have the same formula of OSs detected in the atmosphere, and their precursors were regarded as biogenic VOCs (Kuang et al., 2016; Cai et al., 2020; Wang et al., 2022). For example, previous studies inferred that *m/z* 139 ($C_2H_3O_5S^-$) is produced from isoprene and its derivates related reactions (Cai et al., 2020; Wang et al., 2022). In this study, we found that this compound can also be formed through the oxidation of phenyl sulfate by •OH, providing the additional pathway for its formation in the atmosphere.

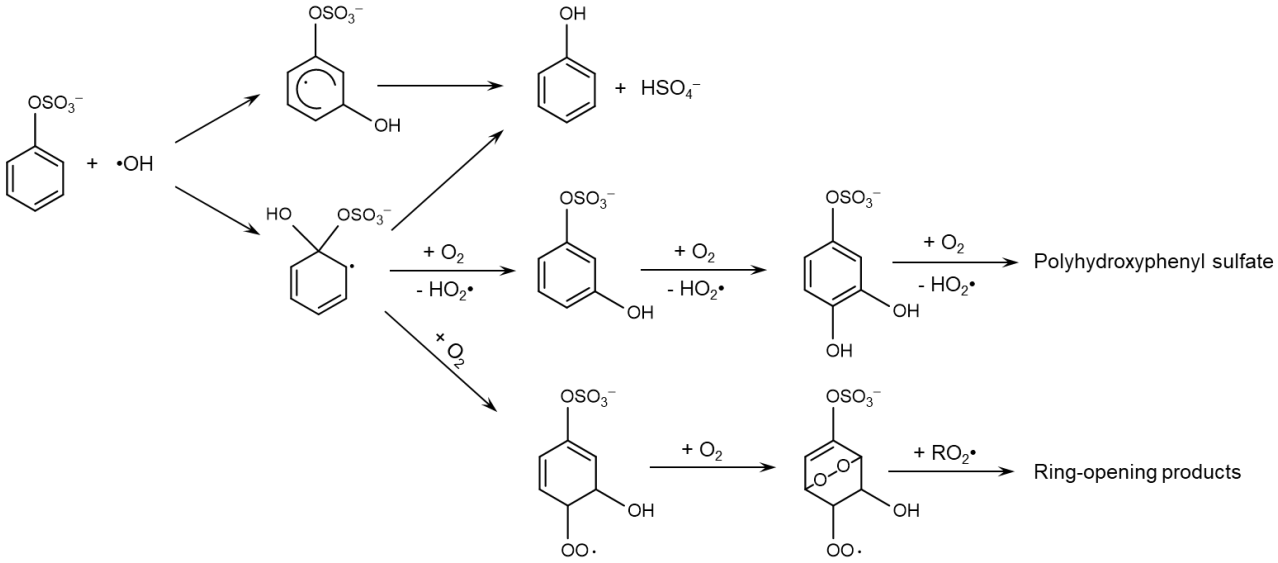

Figure 2. Scheme for the mechanism of phenyl sulfate reacting with •OH.

Previous studies revealed that some aliphatic OSs (e.g., methyl sulfate, ethyl sulfate, 2-methyltetrol sulfate, and α-pinene-derived OS) can be converted into inorganic sulfate during •OH oxidation (Kwong et al., 2018; Xu et al., 2022, 2024; Lai et al., 2025). The reaction is initiated through hydrogen abstraction from the alkyl group, forming an alkyl radical (R•) followed by rapidly reacting with O_2 to form RO_2•. The self- or cross-reactions of RO_2• can further produce an alkoxy radical (RO•). Typically, the formation of inorganic sulfate results from the production of $•SO_4^-$, which is generated from the decomposition of α-OSO_3^- alkoxy radical (defined as the containing of -OSO_3^- group at the α-position of RO•). Additionally, a recent study proposed an alternative mechanism for the formation of inorganic sulfate, proceeding via sulfite radicals ($•SO_3^-$) (Xu et al., 2024). In this pathway, a β-OSO_3^- alkoxy radical (-C(O•)–C(OSO_3^-)-) undergoes C–C bond cleavage, yielding an α-OSO_3^- alkyl radical, subsequently generating non-sulfate products and $•SO_3^-$. Upon the formation of $•SO_4^-$ and $•SO_3^-$, inorganic sulfate can be formed through the further reactions of these radicals. In this study, the formation of inorganic sulfate during the reaction of phenyl sulfate with •OH was also examined. Figure S6a shows that the SO_4^{2-} peak in IC increased progressively with reaction time. The formation of inorganic sulfate was further supported by the evidence of the observed prominent HSO_4^- peak at *m/z* 97, which is assigned to HSO_4^- in the mass spectra. The intensity in the extracted ion chromatograms (EIC) was substantially higher than in dark controls (Fig. S6b), ruling out in-source fragmentation or hydrolysis as the source of HSO_4^-. The results of IC and mass spectrometry suggest that in addition to new OSs, inorganic sulfate can be formed during the reaction. The mechanism of inorganic sulfate formation is elucidated to be produced from the elimination of the sulfate group from phenyl sulfate, as well as the *ipso*-addition followed by disproportionation reaction as shown in Fig. 2. Phenyl sulfate can undergo *ipso*-addition to form OH-PS radical, the *ipso*-OH-adduct can either rapidly eliminate HSO_4^-, or undergo bimolecular reactions with other isomers of the OH-PS radical to yield phenol upon elimination of HSO_4^- as well. However, compared to other OH addition pathways (o-add, m-add, and p-add), there is only very little room for the *ipso*-addition. It is

noted that a previous study has shown that benzoic acid can undergo decarboxylation reactions (Singla et al., 2004). Another possible pathway for HSO_4^- production is proposed to occur via the elimination of the sulfate group from phenyl sulfate, as similar to the decarboxylation mechanism of benzoic acid.

Tables S3 and S4 summarize the identified products from the liquid-phase reactions of p-tolyl sulfate and 4-ethylphenyl sulfate with •OH, respectively. The mechanisms of p-tolyl sulfate and 4-ethylphenyl sulfate oxidized by •OH are similar to that of phenyl sulfate as mentioned above. Similar to phenyl sulfate, the addition of •OH to the aromatic ring predominantly yields phenolic compounds, such as $C_7H_5O_5S^-$, $C_7H_7O_5S^-$, $C_8H_9O_5S^-$, and $C_8H_9O_6S^-$. Further oxidation initiated by hydrogen abstraction can also generate fragmented products, such as $C_5H_5O_6S^-$ and $C_4H_5O_7S^-$ (Tables S3 and S4). Moreover, the presence of alkyl substituents for p-tolyl sulfate and 4-ethylphenyl sulfate can enable additional hydrogen abstraction pathways (Forstner et al., 1997; Baltaretu et al., 2009; Liu et al., 2017), leading to the formation of aromatic aldehydes (e.g., $C_7H_5O_5S^-$, $C_8H_7O_5S^-$). In addition to new OSs formed, the formation of inorganic sulfate was also observed during the process of either p-tolyl sulfate or 4-ethylphenyl sulfate oxidized by •OH. For p-tolyl sulfate, the gradual increase of the SO_4^{2-} peak with reaction time in IC as well as the pronounced signal of *m/z* 97 (HSO_4^-) observed in mass spectra provide robust evidences for the formation of inorganic sulfate during the reaction (Fig. S7). For 4-ethylphenyl sulfate, SO_4^{2-} peak in IC was found to overlap with that of the compound itself (Fig. S8a). The inference that 4-ethylphenyl sulfate converts to inorganic sulfate is supported by comparing the intensity of HSO_4^- (*m/z* 97) peak of samples collected from illumination and dark conditions (Fig. S8b).

3.3 Optical property changes

Kinetic and mechanism results show that aromatic OSs can undergo rapid •OH oxidation to form a series of functionalized and fragmented compounds. The changes of optical properties resulting from the formation of these compounds were also investigated. Figure S9 shows the time-dependent absorption spectra of aromatic OSs during •OH oxidation at pH 3. As the reaction progressed, the consumption of reactants accompanied by an increase in absorbance across 250–400 nm. To establish the relationship between light absorption and organic compounds, chromophores formed in the reaction were identified by correlating UV absorption bands with the retention time based on UPLC-PAD-MS analysis. For phenyl sulfate, Figures 3a and 3bdisplays that phenyl sulfate (*m/z* 173) was the prominent chromophore with the retention time of 5.67–6.16 min at the beginning of the reaction, exhibiting a characteristic absorption peak at 262 nm (Fig. S10). After the liquid-phase •OH oxidation, five major chromophores were observed as shown in Fig. 3c. Chromophore #4 was assigned to the unreacted phenyl sulfate. Figure 3c shows that Chromophore #1, #2, and #3 eluted at 3.47–3.72 min, 4.00–4.18 min, and 5.46–5.60 min, respectively. These newly formed chromophores exhibit red-shifted absorption peaks (Fig. 10), likely due to the electron-donating effect of hydroxyl groups increasing aromatic ring electron density (Hems and Abbatt, 2018). The results of EIC suggest that these chromophores correspond to co-eluting mixtures containing $C_6H_5O_5S^-$ isomers (*m/z* 189), along with $C_6H_5O_6S^-$ (*m/z* 205), $C_6H_5O_7S^-$ (*m/z* 221) and $C_6H_7O_8S^-$ (*m/z* 239) (Fig. 3d). Among these compounds, $C_6H_5O_6S^-$ exhibited the highest intensity. Chromophore #5, eluting at 14.98–15.67 min, remained unidentified. Its later elution time suggests a

larger molecular structure and lower polarity (Fleming et al., 2020). Additionally, there may exist other chromophores unidentified since these five chromophores cannot fully explain the total light adsorption as shown in Fig. S10.

For p-tolyl sulfate, the increase in absorbance, contributing by the formation of chromophores, was also observed after •OH oxidation. The primarily newly formed chromophore (Chromophore #1), eluting at 5.23–5.78 min, was identified as $C_7H_5O_5S^-$ (*m/z* 201) based on the corresponding EIC (Figs. S11). A blue-shift peak at 258 nm was observed upon the formation of $C_7H_5O_5S^-$, which is associated with the generation of a carbonyl (C=O) functional group (Fig. S12). Other newly formed chromophores were characterized as Chromophore #2 and Chromophore #3. Chromophore #2 corresponded to a mixture of $C_7H_7O_5S^-$ (*m/z* 203), $C_7H_5O_6S^-$ (*m/z* 217), and $C_7H_7O_6S^-$ (*m/z* 219) with absorption band at 274 nm, and Chromophore #3 was assigned to an isomer of $C_7H_7O_5S^-$ (*m/z* 203) with the absorption band at 266 nm (Figs. S11 and S12). Figures S13 and S14 show the characterization of chromophores formed from liquid-phase reaction of 4-ethylphenyl sulfate with OH radicals. After reactions, Chromophore #2 ($C_8H_7O_5S^-$, *m/z* 215) with a characteristic absorption peak at 254 nm was the dominant contributor to total light absorption. Four additional chromophores were also identified: Chromophore #1, a mixture of $C_7H_7O_5S^-$ (*m/z* 201), $C_8H_9O_5S^-$ (*m/z* 217), $C_8H_7O_6S^-$ (*m/z* 231), and $C_8H_9O_6S^-$ (*m/z* 233), with absorption peak at 258 nm; Chromophore #3, an isomer of $C_8H_7O_6S^-$, with absorption peak at 262 nm; Chromophore #4, an isomer of $C_8H_9O_5S^-$ (*m/z* 217), with absorption peak at 274 nm; and Chromophore #5, another isomer of $C_8H_9O_5S^-$, also with a characteristic absorption peak at 274 nm.

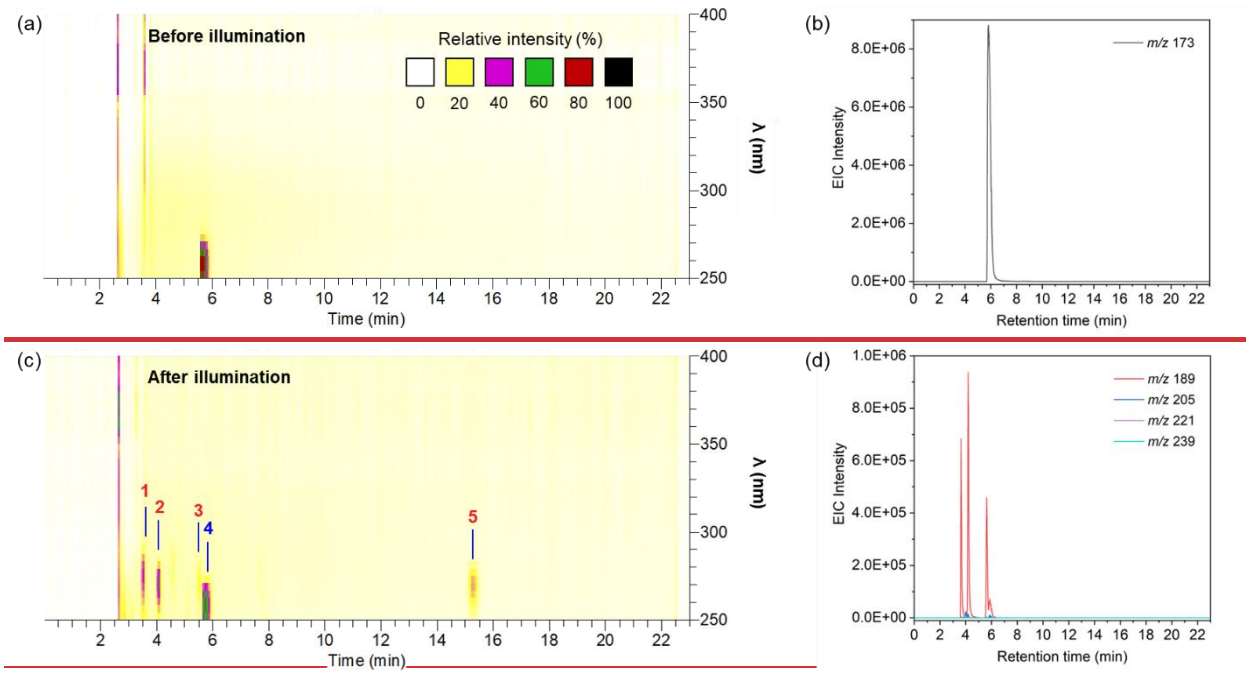

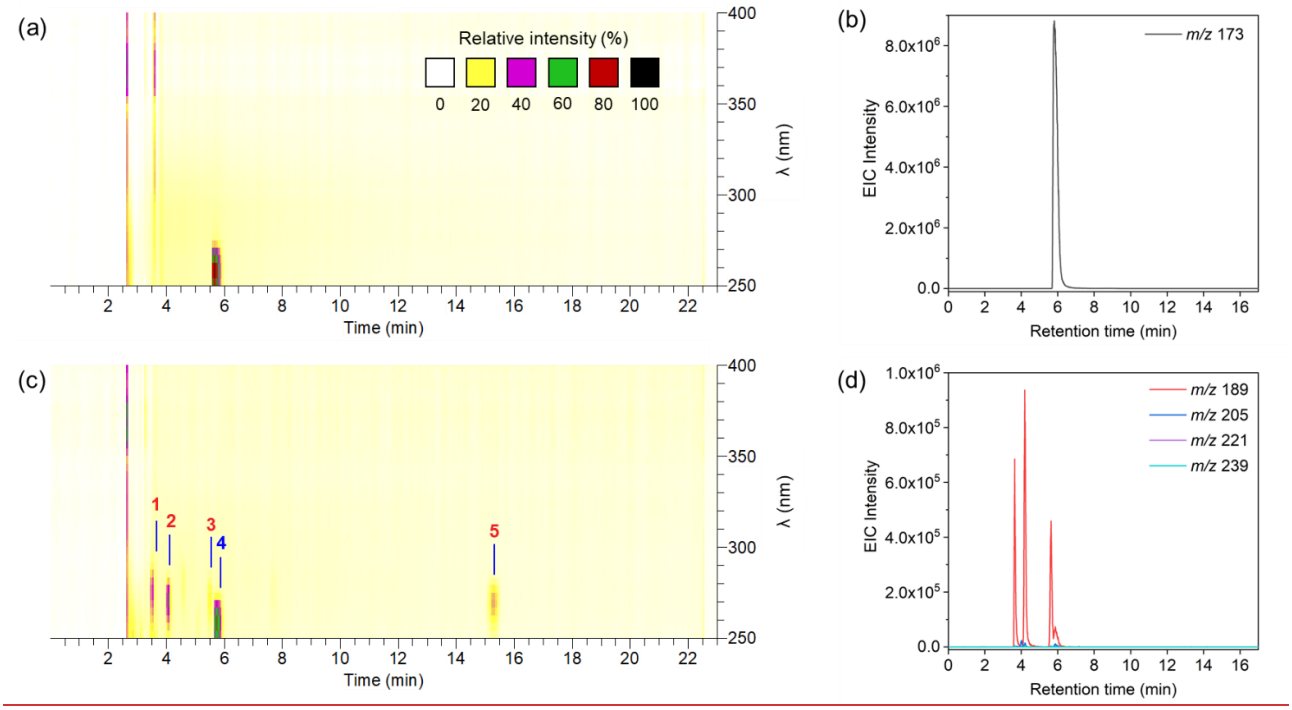

Figure 3. UPLC-PAD-MS chromatograms of samples collected (a) before and (c) after the liquid-phase •OH oxidation of phenyl sulfate at pH 3. The y-axis and color map represents the wavelength and corresponding UV-vis absorbance, respectively. Extracted ion chromatograms (EIC) of (b) phenyl sulfate and (d) the compositions of chromophores.

Furthermore, fluorescence evolutions during liquid-phase •OH oxidation of aromatic OSs were investigated as shown in Fig. 4. The initial maximum excitation/emission (Ex/Em) wavelengths of phenyl sulfate, p-tolyl sulfate, and 4-ethylphenyl sulfate at pH 3 were Ex/Em = 255/275 nm, 260/284 nm, and 260/284 nm, respectively. The different initial fluorescence intensity among these three aromatic OSs may be attributed to the substituent effect of the compound. Compared to phenyl sulfate, p-tolyl sulfate and 4-ethylphenyl sulfate contain additional methyl and ethyl groups, respectively. These electron-donating substituents extend the conjugation system, lowering the π→π* transition energy and resulting in both emission redshift and fluorescence enhancement (Cao et al., 2023). During the reaction, the fluorescence intensity initially decreased due to phenyl sulfate consumption, followed by an increase from fluorescent product formation. After 8 h of illumination, a redshifted fluorescence peak emerged at Ex/Em = 260/283 nm, implying the formation of products with expanded conjugated systems (e.g., $C_6H_5O_5S^-$, $C_6H_5O_6S^-$, and $C_6H_5O_7S^-$) (Tang et al., 2020). The fluorescence intensity of p-tolyl sulfate and 4-ethylphenyl sulfate monotonically decreased with the reaction time and showed a redshift in the fluorescence band at Ex/Em = (250–300)/(400–500). Previous studies uncovered that the emission wavelengths of 400–500 nm are indicative of humic-like substances (HULIS), which can significantly contribute to the light-absorbing properties of organic aerosols (Bianco et al., 2014). Previous studies revealed that the oxidation of non-photolyzable phenolics by •OH can yield HULIS-like fluorescent products (Tang et al., 2020; Chang et al., 2010). Here, multi-hydroxy products from p-tolyl sulfate (e.g., $C_7H_7O_5S^-$, $C_7H_7O_6S^-$

and $C_7H_7O_7S^-$) and 4-ethylphenyl sulfate (e.g., $C_8H_9O_5S^-$, $C_8H_9O_6S^-$, and $C_8H_9O_7S^-$) may exhibit spectral features resembling aerosol HULIS.

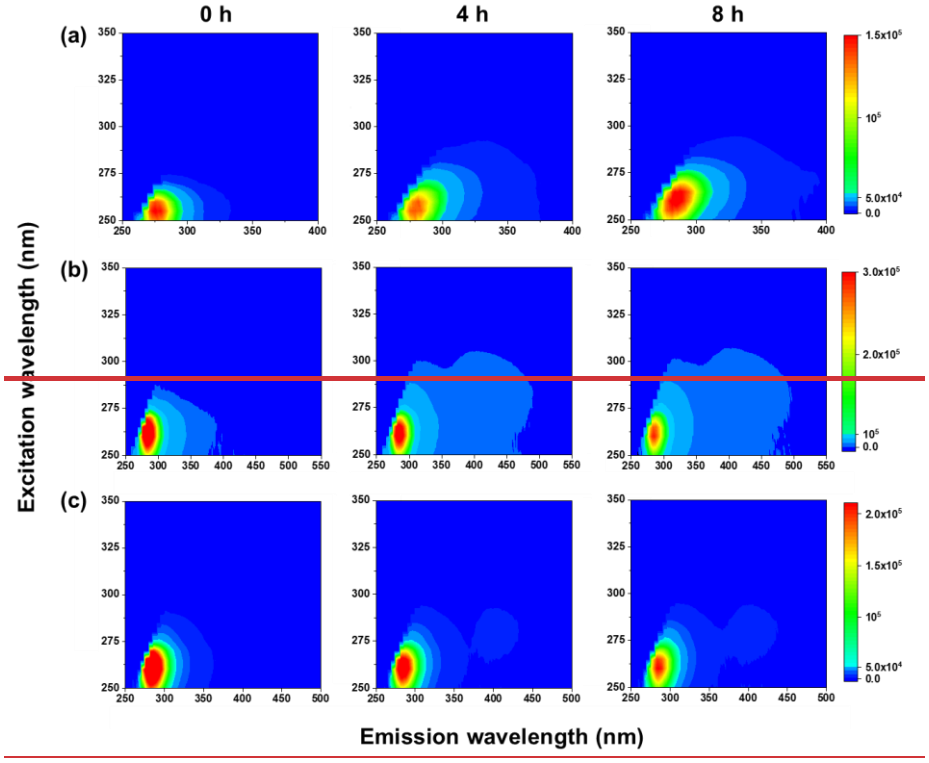

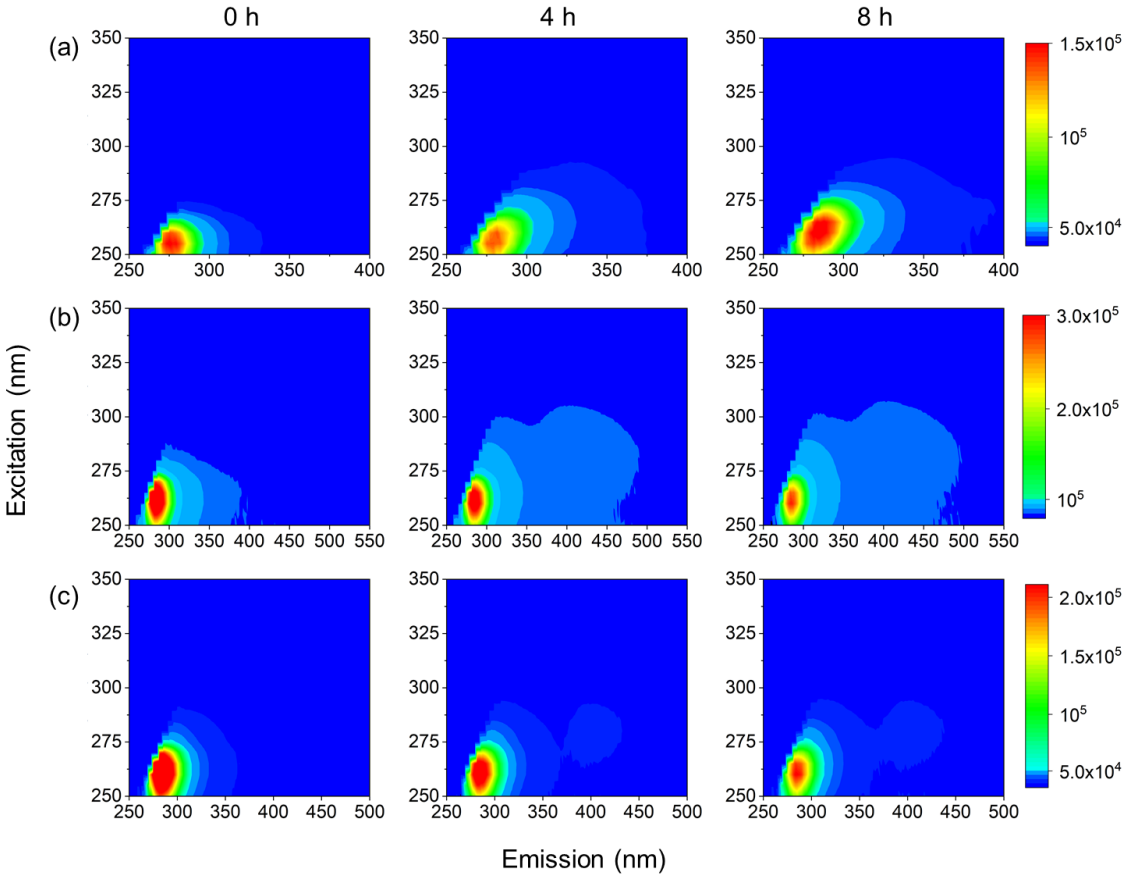

Figure 4. Time profile of excitation–emission matrix (EEM) fluorescence spectra during the processes of (a) phenyl sulfate, (b) p-tolyl sulfate and (c) 4-ethylphenyl sulfate reacting with •OH at pH 3.

Employing phenyl sulfate as the representative, spectral changes at pH 8 were also examined. Previous studies have demonstrated that the light absorption properties of carbonyl compounds (e.g., aldehydes) and nitrophenols exhibit pronounced pH-dependence owing to protonation-deprotonation equilibria (Calvert and Schnitzler, 2023; Chen et al., 2020a). In this study, phenyl sulfate remains deprotonated across the pH range of 3–8, resulting in negligible spectral variations in the initial solution (Figs. S9a and S15). However, the temporal evolution of the reaction revealed substantially enhanced absorbance at pH 3 compared to pH 8, particularly within the 300–400 nm range. Figure S16 shows the molecular composition of chromophores from the reaction of phenyl sulfate with •OH at pH 8. Chromophores #1–3 were identical to those at pH 3 but exhibited stronger absorption due to their higher concentrations. An additional chromophore #4, eluting at 4.99–5.23 min, contributed significantly to absorption but the detailed composition of this chromophore is unknown. Compared to pH 3, solution at pH 8 exhibited an enhanced peak intensity at 4.99–5.23 min, while the peak at 14.98–15.67 min was reduced, which corresponded to distinct changes in the relative contributions to total absorption. For fluorescence spectra, phenyl sulfate exhibited an initial maximum fluorescence peak at Ex/Em = 255/279 nm at pH 8 (Fig. S17), displaying minimal variation from the pH 3 conditions

(Fig. 4a). However, the temporal evolution of its fluorescence spectrum differs obviously at different pH values. Under basic conditions (pH 8), fluorescence decreased monotonically without recovery and no red shift occurred even after 8 h.

4 Atmospheric implications and conclusions

The current study investigated the liquid-phase reactions of three aromatic OSs (i.e., phenyl sulfate, p-tolyl sulfate, and 4-ethylphenyl sulfate) with •OH. It is found that functionalized and fragmented OSs as well as inorganic sulfate can be yielded during the reactions. The formation of functionalized OSs can enhance light absorption, thereby influencing aerosol optical properties. Fragmented OS formation resulting from ring-opening pathways during •OH oxidation of aromatic OSs has not been reported previously. Several fragmented OSs (e.g., $C_2H_3O_5S^-$, $C_5H_7O_8S^-$, $C_4H_5O_7S^-$, and $C_5H_5O_6S^-$) detected in our study have been previously identified in ambient aerosols (Kuang et al., 2016; Cai et al., 2020; Wang et al., 2022; Yang et al., 2023), suggesting that aromatic OSs may serve as a potential source for aliphatic OSs in the atmosphere. Furthermore, the observation of inorganic sulfate formation, for the first time, indicates that aromatic OSs can also be converted into inorganic sulfate in analogous to aliphatic OSs (Kwong et al., 2018; Xu et al., 2022, 2024; Lai et al., 2025), potentially contributing to the atmospheric sulfur cycle. Further investigations are warranted to examine whether the proposed mechanism can be also applied to other types of aromatic OSs in the atmosphere.

The results of kinetic measurements reveal that aromatic OSs can react rapidly with •OH. As shown in Table S5, using the k values coupled with modeled •OH concentrations (Herrmann et al., 2005, 2010), the corresponding lifetimes ($\tau = 1/k_{OS} \times [\bullet OH]$) of aromatic OSs can be calculated. In urban areas, the concentration of •OH in cloud and aerosols was estimated as 3.5×10^{-15} and 4.4×10^{-13} M, respectively. In contrast to urban areas, remote areas exhibit higher •OH concentrations both in cloud (2.2×10^{-14} M) and aerosols (3.0×10^{-12} M) (Herrmann et al., 2005, 2010). Concentrations of •OH are consistently higher in aerosols than in cloud across different environments. Consequently, the lifetimes of aromatic OSs ranged from approximately 1 min in remote aerosols to up to 16 h in urban cloud water (Table S5), highlighting the significant influence of environmental conditions on their persistence. Previous studies reported that the lifetimes of aliphatic OSs in such varied environments range from several minutes to dozen days (Gweme and Styler, 2024; Lai et al., 2025). The substantially shorter lifetimes of aromatic OSs can be attributed to their higher reactivity toward •OH compared to aliphatic OSs. Given the high abundance of aromatic OSs and their fast k_{OS} values in urban environments, aromatic OSs likely play a significant role in both the atmospheric sulfur cycle and environmental effects. In addition to lifetimes in aqueous environments, previous studies also estimated the atmospheric lifetimes of several aliphatic OSs via heterogeneous •OH oxidation based on measured uptake coefficients (Kwong et al., 2018; Lam et al., 2019; Xu et al., 2022). For instance, the atmospheric lifetime of methyl sulfate ranges from 53 min to 32 days via liquid-phase •OH oxidation, compared to approximately 20 days via heterogeneous •OH oxidation (Gweme and Styler, 2024; Kwong et al., 2018). The results indicate that the atmospheric lifetimes of these OSs differ between liquid-phase and heterogeneous •OH oxidation pathways. However, experiments of heterogeneous reactions of aromatic OSs

with •OH were not performed in this study. Thus, we cannot directly compare the lifetime of aromatic and aliphatic OSs through heterogeneous •OH oxidation, and need further investigation.

Data availability. Data are available upon request from the corresponding author.

Supplement. The supplement related to this article is available online.

Author contributions. LH designed research. YY, CY RY, PL, HZ, and HC, performed research. YY and LH analyzed data. YY and LH wrote the paper. LX, CY, YW, YZ, and HS provided valuable comments and suggestions for the manuscript.

Competing interests. The contact author has declared that none of the authors has any competing interests.

Acknowledgements. This study was financially supported by the National Key Research and Development Program of China (2022YFC3701102), the National Natural Science Foundation of China (42207121), the Outstanding Young Scholar of the Natural Science Foundation of Shandong Province, China (Overseas) (2022HWYQ-010), the Natural Science Foundation of Shandong Province (ZR2024YQ046). Liubin Huang gratefully acknowledges the support of the Program for Taishan Young Scholar (tsqnz20221107).

References

Arciva, S., Niedek, C., Mavis, C., Yoon, M., Sanchez, M. E., Zhang, Q., and Anastasio, C.: Aqueous •OH oxidation of highly substituted phenols as a source of secondary organic aerosol, Environ. Sci. Technol., 56, 9959–9967, https://doi.org/10.1021/acs.est.2c02225, 2022.

Arciva, S., Ma, L., Mavis, C., Guzman, C., and Anastasio, C.: Formation and loss of light absorbance by phenolic aqueous SOA by •OH and an organic triplet excited state, Atmos. Chem. Phys., 24, 4473–4485, https://doi.org/10.5194/acp-24-4473-2024, 2024.

Baltaretu, C. O., Lichtman, E. I., Hadler, A. B., and Elrod, M. J.: Primary atmospheric oxidation mechanism for toluene, J. Phys. Chem. A, 113, 221–230, https://doi.org/10.1021/jp806841t, 2009.

Bianco, A., Minella, M., Laurentiis, E. D., Maurino, V., Minero, C., and Vione, D.: Photochemical generation of photoactive compounds with fulvic-like and humic-like fluorescence in aqueous solution, Chemosphere, 111, 529–536, https://doi.org/10.1016/j.chemosphere.2014.04.035, 2014.

Bloss, C., Wagner, V., Jenkin, M. E., Volkamer, R., Bloss, W. J., Lee, J. D., Heard, D. E., Wirtz, K., Martin-Reviejo, M., Rea, G., Wenger, J. C., and Pilling, M. J.: Development of a detailed chemical mechanism (MCMv3.1) for the atmospheric oxidation of aromatic hydrocarbons, Atmos. Chem. Phys., 5, 641–664, https://doi.org/10.5194/acp-5-641-2005, 2005.

Buxton, G. V., Greenstock, C. L., Helman, W. P., and Ross, A. B.: Critical review of rate constants for reactions of hydrated electrons, hydrogen atoms and hydroxyl radicals (•OH/•O^- in aqueous solution, J. Phys. Chem. Ref. Data, 17, 513–886, https://doi.org/10.1063/1.555805, 1988.

Cai, D., Wang, X., Chen, J., and Li, X.: Molecular characterization of organosulfates in highly polluted atmosphere using ultra-high-resolution mass spectrometry, J. Geophys. Res.: Atmos., 125, e2019JD032253, https://doi.org/10.1029/2019JD032253, 2020.

Calvert, C. T., and Schnitzler, E. G.: Light absorption by cinnamaldehyde constituents of biomass burning organic aerosol modeled using time-dependent density functional theory, ACS Earth Space Chem., 7, 490–500, https://doi.org/10.1021/acsearthspacechem.2c00344, 2023.

Cao, T., Li, M., Xu, C., Song, J., Fan, X., Li, J., Jia, W., and Peng, P.: Technical note: Chemical composition and source identification of fluorescent components in atmospheric water-soluble brown carbon by excitation–emission matrix spectroscopy with parallel factor analysis – potential limitations and applications, Atmos. Chem. Phys., 23, 2613–2625, https://doi.org/10.5194/acp-23-2613-2023, 2023.

Chang, J. L., and Thompson, J. E.: Characterization of colored products formed during irradiation of aqueous solutions containing H_2O_2 and phenolic compounds, Atmos. Environ., 44, 541–551, https://doi.org/10.1016/j.atmosenv.2009.10.042, 2010.

Chen, J. Y., Rodriguez, E., Jiang, H., Chen, K., Frie, A., Zhang, H., Bahreini, R., and Lin, Y-H.: Time-dependent density functional theory investigation of the UV–Vis spectra of organonitrogen chromophores in brown carbon, ACS Earth Space Chem., 4, 311–320, https://doi.org/10.1021/acsearthspacechem.9b00328, 2020a.Chen, Y., Zhang, Y., Lambe, A. L., Xu, R., Lei, Z., Olson, N. E., Zhang, Z., Szalkowski, T., Cui, T., Vizuete, W., Gold, A., Turpin, B. J., Ault, A. P., Chan, M. N., Surratt, J. D.: Heterogeneous hydroxyl radical oxidation of isoprene-epoxydiol-derived methyltetrol sulfates: Plausible formation mechanisms of previously unexplained organosulfates in ambient fine aerosols, Environ. Sci. Technol. Lett., 7, 460–468, https://doi.org/10.1021/acs.estlett.0c00276, 2020b.

Darer, A. I., Cole-Filipiak, N. C., O'Connor, A. E., and Elrod, M. J.: Formation and stability of atmospherically relevant isoprene-derived organosulfates and organonitrates, Environ. Sci. Technol., 45, 1895–1902, https://doi.org/10.1021/es103797z, 2011.

Dong, P., Chen, Z., Qin, X., and Gong, Y.: Water significantly changes the ring-cleavage process during aqueous photooxidation of toluene, Environ. Sci. Technol., 55, 16316–16325, https://doi.org/10.1021/acs.est.1c04770, 2021.

Dorfman, L. M., and Adams, G. E.: Reactivity of the hydroxyl radical in aqueous solutions, National Bureau of Standards, 76, 1973.

Forstner, H. J. L., Flagan, R. C., and Seinfeld, J. H.: Secondary organic aerosol from the photooxidation of aromatic hydrocarbons: Molecular composition, Environ. Sci. Technol., 31, 1345–1358, https://doi.org/10.1021/es9605376, 1997.

Garmash, O., Rissanen, M. P., Pullinen, I., Schmitt, S., Kausiala, O., Tillmann, R., Zhao, D., Percival, C., Bannan, T. J., Priestley, M., Hallquist, Å. M., Kleist, E., Kiendler-Scharr, A., Hallquist, M., Berndt, T., McFiggans, G., Wildt, J., Mentel, T. F., and Ehn, M.: Multi-generation OH oxidation as a source for highly oxygenated organic molecules from aromatics, Atmos. Chem. Phys., 20, 515–537, https://doi.org/10.5194/acp-20-515-2020, 2020.

Gweme, D. T., and Styler, S. A.: OH radical oxidation of organosulfates in the atmospheric aqueous phase, J. Phys. Chem. A,

128, 9462–9475, https://doi.org/10.1021/acs.jpca.4c02877, 2024.

Hansen, A. M. K., Kristensen, K., Nguyen, Q. T., Zare, A., Cozzi, F., Nøjgaard, J. K., Skov, H., Brandt, J., Christensen, J. H., Ström, J., Tunved, P., Krejci, R., and Glasius, M.: Organosulfates and organic acids in Arctic aerosols: speciation, annual variation and concentration levels, Atmos. Chem. Phys., 14, 7807–7823, https://doi.org/10.5194/acp-14-7807-2014, 2014.

Harrison, A. W., Waterson, A. M., and De Bruyn, W. J.: Spectroscopic and photochemical properties of secondary brown carbon from aqueous reactions of methylglyoxal, ACS Earth Space Chem., 4, 762–773, https://doi.org/10.1021/acsearthspacechem.0c00061, 2020.

He, J., Li, L., Li, Y., Huang, M., Zhu, Y., and Deng, S.: Synthesis, MS/MS characteristics and quantification of six aromatic organosulfates in atmospheric $PM_{2.5}$, Atmos. Environ., 290, 119361, https://doi.org/10.1016/j.atmosenv.2022.119361, 2022.

Heath, A. A., Ehrenhauser, F. S., and Valsaraj, K. T.: Effects of temperature, oxygen level, ionic strength, and pH on the reaction of benzene with hydroxyl radicals in aqueous atmospheric systems, Environ. Chem. Eng., 1, 822–830, https://doi.org/10.1016/j.jece.2013.07.023, 2013.

Hems, R. F., and Abbatt, J. P. D.: Aqueous phase photo-oxidation of brown carbon nitrophenols: Reaction kinetics, mechanism, and evolution of light absorption, ACS Earth Space Chem., 2, 225–234, https://doi.org/10.1021/acsearthspacechem.7b00123, 2018.

Herrmann, H., Tilgner, A., Barzaghi, P., Majdik, Z., Gligorovski, S., Poulain, L., and Monod, A.: Towards a more detailed description of tropospheric aqueous phase organic chemistry: CAPRAM 3.0, Atmos. Environ., 39, 4351–4363, https://doi.org/10.1016/j.atmosenv.2005.02.016, 2005.

Herrmann, H., Hoffmann, D., Schaefer, T., Bräuer, P., and Tilgner, A.: Tropospheric aqueous-phase free-radical chemistry: Radical sources, spectra, reaction kinetics and prediction tools, Chem. Phys. Chem., 11, 3796–3822, https://doi.org/10.1002/cphc.201000533, 2010.

Herrmann, H., Schaefer, T., Tilgner, A., Styler, S. A., Weller,C., Teich, M., and Otto, T.: Tropospheric aqueous-phase chemistry: Kinetics, mechanisms, and its coupling to a changing gas phase, Chem. Rev., 115, 4259–4334, https://doi.org/10.1021/cr500447k, 2015.

Hettiyadura, A. P. S., Jayarathne, T., Baumann, K., Goldstein, A. H., de Gouw, J. A., Koss, A., Keutsch, F. N., Skog, K., and Stone, E. A.: Qualitative and quantitative analysis of atmospheric organosulfates in Centreville, Alabama, Atmos. Chem. Phys., 17, 1343–1359, https://doi.org/10.5194/acp-17-1343-2017, 2017.

Hettiyadura, A. P. S., Al-Naiema, I. M., Hughes, D. D., Fang, T., and Stone, E. A.: Organosulfates in Atlanta, Georgia: anthropogenic influences on biogenic secondary organic aerosol formation, Atmos. Chem. Phys., 19, 3191–3206, https://doi.org/10.5194/acp-19-3191-2019, 2019.

Hu, K. S., Darer, A. I., and Elrod, M. J.: Thermodynamics and kinetics of the hydrolysis of atmospherically relevant organonitrates and organosulfates, Atmos. Chem. Phys., 11, 8307–8320, https://doi.org/10.5194/acp-11-8307-2011, 2011.

Hu, W. W., Campuzano-Jost, P., Palm, B. B., Day, D. A., Ortega, A. M., Hayes, P. L., Krechmer, J. E., Chen, Q., Kuwata, M.,

Liu, Y. J., de Sá, S. S., McKinney, K., Martin, S. T., Hu, M., Budisulistiorini, S. H., Riva, M., Surratt, J. D., St. Clair, J. M., Isaacman-Van Wertz, G., Yee, L. D., Goldstein, A. H., Carbone, S., Brito, J., Artaxo, P., de Gouw, J. A., Koss, A., Wisthaler, A., Mikoviny, T., Karl, T., Kaser, L., Jud, W., Hansel, A., Docherty, K. S., Alexander, M. L., Robinson, N. H., Coe, H., Allan, J. D., Canagaratna, M. R., Paulot, F., and Jimenez, J. L.: Characterization of a real-time tracer for isoprene epoxydiols-derived secondary organic aerosol (IEPOX-SOA) from aerosol mass spectrometer measurements, Atmos. Chem. Phys., 15, 11807–11833, https://doi.org/10.5194/acp-15-11807-2015, 2015.

Huang, L., Cochran, R. E., Coddens, E. M., and Grassian, V. H.: Formation of organosulfur compounds through transition metal ion-catalyzed aqueous phase reactions, Environ. Sci. Technol. Lett., 5, 315–321, https://doi.org/10.1021/acs.estlett.8b00225, 2018.

Huang, L., Wang, Y., Zhao, Y., Hu, H., Yang, Y., Wang, Y., Yu, J-Z., Chen, T., Cheng, Z., Li, C., and Xiao., H.: Biogenic and anthropogenic contributions to atmospheric organosulfates in a typical megacity in eastern China, J. Geophys. Res.: Atmos., 128, e2023JD038848, https://doi.org/10.1029/2023JD038848, 2023.

Iinuma, Y., Müller, C., Berndt, T., Böge, O., Claeys, M., and Herrmann, H.: Evidence for the existence of organosulfates from β-Pinene ozonolysis in ambient secondary organic aerosol, Environ. Sci. Technol., 41, 6678–6683, https://doi.org/10.1021/es070938t, 2007.

Kuang, B. Y., Lin, P., Hu, M., and Yu, J. Z.: Aerosol size distribution characteristics of organosulfates in the Pearl River Delta region, China, Atmos. Environ., 130, 23–35, https://doi.org/10.1016/j.atmosenv.2015.09.024, 2016.

Kundu, S., Quraishi, T. A., Yu, G., Suarez, C., Keutsch, F. N., and Stone, E. A.: Evidence and quantitation of aromatic organosulfates in ambient aerosols in Lahore, Pakistan, Atmos. Chem. Phys., 13, 4865–4875, https://doi.org/10.5194/acp-13-4865-2013, 2013.

Kwong, K. C., Chim, M. M., Davies, J. F., Wilson, K. R., and Chan, M. N.: Importance of sulfate radical anion formation and chemistry in heterogeneous •OH oxidation of sodium methyl sulfate, the smallest organosulfate, Atmos. Chem. Phys., 18, 2809–2820, https://doi.org/10.5194/acp-18-2809-2018, 2018.

Kristensen, K., and Glasius, M.: Organosulfates and oxidation products from biogenic hydrocarbons in fine aerosols from a forest in north west Europe during spring, Atmos. Environ., 45, 4546–4556, https://doi.org/10.1016/j.atmosenv.2011.05.063, 2011.

Lai, D., Schaefer, T., Zhang, Y., Li, Y. J., Xing, S., Herrmann, H., and Chan, M. N.: Deactivating effect of hydroxyl radicals reactivity by sulfate and sulfite functional groups in aqueous phase─atmospheric implications for small organosulfur compounds, ACS EST Air, 1, 678–689, https://doi.org/10.1021/acsestair.4c00033, 2024.

Lai, D., Bai, Y., Zhang, Z., So, P.-K., Li, Y. J., Tse, Y.-L. S., Yeung, Y.-Y., Schaefer, T., Herrmann, H., Yu, J. Z., Wang, Y., and Chan, M. N.: Rapid aqueous-phase oxidation of an α-pinene-derived organosulfate by hydroxyl radicals: a potential source of some unclassified oxygenated and small organosulfates in the atmosphere, Atmos. Chem. Phys., 25, 12569–12584, https://doi.org/10.5194/acp-25-12569-2025, 2025.

Laskin, A., Laskin, J., and Nizkorodov, S. A.: Chemistry of atmospheric brown carbon, Chem. Rev., 115, 4335–4382,

https://doi.org/10.1021/cr5006167, 2015.

Lay, T. H., Bozzelli, J. W., and Seinfeld, J. H.: Atmospheric photochemical oxidation of benzene: benzene + OH and the benzene−OH adduct (hydroxyl-2,4-cyclohexadienyl) + O_2, J. Phys. Chem., 100, 6543–6554, https://doi.org/10.1021/jp951726y, 1996.

Lei, Z., Chen, Y., Zhang, Y., Cooke, M. E., Ledsky, I. R., Armstrong, N. C., Olson, N. E., Zhang, Z., Gold, A., Surratt, J. D., and Ault, A. P.: Initial pH governs secondary organic aerosol phase state and morphology after uptake of isoprene epoxydiols (IEPOX), Environ. Sci. Technol., 56, 10596–10607, https://doi.org/10.1021/acs.est.2c01579, 2022.

Li, F., Tsona, N. T., Li, J., and Du, L.: Aqueous-phase oxidation of syringic acid emitted from biomass burning: Formation of light-absorbing compounds, Sci. Total Environ., 765, 144239, https://doi.org/10.1016/j.scitotenv.2020.144239, 2021.

Liu, F., Xu, T., Ng, N. L., and Lu, H.: Linking cell health and reactive oxygen species from secondary organic aerosols exposure, Environ. Sci. Technol., 57, 1039–1048, https://doi.org/10.1021/acs.est.2c05171, 2022.

Li, S., Wang, Y., Zhang, Y., Yi, Y., Wang, Y., Guo, Y., Yu, C., Jiang, Y., Shi, J., Zhang, C., Zhu, J., Hu, W., Yu, J., Yao, X., Gao, H., and Hu, M.: Atmospheric organosulfate formation regulated by continental outflows and marine emissions over East Asian marginal seas, Atmos. Chem. Phys., 25, 12585–12598, https://doi.org/10.5194/acp-25-12585-2025, 2025.

Liu, G., Ji, J., Huang, H., Xie, R., Feng, Q., Shu, Y., Zhan, Y., Fang, R., He, M., Liu, S., Ye, X., and Leung, D. Y. C.: UV/H_2O_2: An efficient aqueous advanced oxidation process for VOCs removal, Chem. Eng. J., 324, 44–50, https://doi.org/10.1016/j.cej.2017.04.105, 2017.

Lin, Y.-H., Knipping, E. M., Edgerton, E. S., Shaw, S. L., and Surratt, J. D.: Investigating the influences of SO_2 and NH_3 levels on isoprene-derived secondary organic aerosol formation using conditional sampling approaches, Atmos. Chem. Phys., 13, 8457–8470, https://doi.org/10.5194/acp-13-8457-2013, 2013.

Lukács, H., Gelencsér, A., Hoffer, A., Kiss, G., Horváth, K., and Hartyáni, Z.: Quantitative assessment of organosulfates in size-segregated rural fine aerosol, Atmos. Chem. Phys., 9, 231–238, https://doi.org/10.5194/acp-9-231-2009, 2009.

Ma, J., Reininger, N., Zhao, C, Döbler, D., Rüdiger, J., Qiu, Y., Ungeheuer, F., Simon, M., D'Angelo, L., Breuninger, A., David, J., Bai, Y., Li, Y., Xue, Y., Li, L., Wang, Y., Hildmann, S., Hoffmann, T., Liu, B., Niu, H., Wu, Z., and Vogel, A. L.: Unveiling a large fraction of hidden organosulfates in ambient organic aerosol, Nat. Commun., 16, 4098, https://doi.org/10.1038/s41467-025-59420-y, 2025.

Ma, Y., Xu, X., Song, W., Geng, F., and Wang, L.: Seasonal and diurnal variations of particulate organosulfates in urban Shanghai, China, Atmos. Environ., 85, 152–160, https://doi.org/10.1016/j.atmosenv.2013.12.017, 2014.

Mael, L. E., Jacobs, M. I., and Elrod, M. J.: Organosulfate and nitrate formation and reactivity from epoxides derived from 2-Methyl-3-buten-2-ol, J. Phys. Chem. A, 119, 4464–4472, https://doi.org/10.1021/jp510033s, 2015.

Minakata, D., Song, W., Mezyk, S. P., and Cooper, W. J.: Experimental and theoretical studies on aqueous-phase reactivity of hydroxyl radicals with multiple carboxylated and hydroxylated benzene compounds, Phys. Chem. Chem. Phys., 17, 11796–11812, https://doi.org/10.1039/C5CP00861A, 2015.

Minerath, E. C., Casale, M. T., and Elrod, M. J.: Kinetics feasibility study of alcohol sulfate esterification reactions in

tropospheric aerosols, Environ. Sci. Technol., 42, 4410–4415, https://doi.org/10.1021/es8004333, 2008.

Monod, A., and Doussin, J. F.: Structure-activity relationship for the estimation of OH-oxidation rate constants of aliphatic organic compounds in the aqueous phase: alkanes, alcohols, organic acids and bases, Atmos. Environ., 42, 7611-7622, https://doi.org/10.1016/j.atmosenv.2008.06.005, 2008.

Nozière, B., Ekström, S., Alsberg, T., and Holmström S.: Radical-initiated formation of organosulfates and surfactants in atmospheric aerosols, Geophys. Res. Lett., 37, L05806, https://doi.org/10.1029/2009GL041683, 2010.

Pan, X-M., Schuchmann, M. N., and Sonntag, C. V.: Oxidation of benzene by the OH radical. A product and pulse radiolysis study in oxygenated aqueous solution, J. Chem. Soc., Perkin Trans., 2, 289–297, https://doi.org/10.1039/P29930000289, 1993.

Passananti, M., Kong, L., Shang, J., Dupart, Y., Perrier, S., Chen, J., Donaldson, J., and George, C.: Organosulfate formation through the heterogeneous reaction of sulfur dioxide with unsaturated fatty acids and long-chain alkenes, Angew. Chem. Int. Ed., 55, 10336-10339, https://doi.org/10.1002/anie.201605266, 2016.

Peng, X., Xie, T-T., Tang, M-X., Cheng, Y., Peng, Y., Wei, F-H., Cao, L-M., Yu, K., Du, K., He, L-Y., and Huang, X-F.: Critical role of secondary organic aerosol in urban atmospheric visibility improvement identified by machine learning, Environ. Sci. Technol. Lett., 10, 976–982, https://doi.org/10.1021/acs.estlett.3c00084, 2023.

Pye, H. O. T., Nenes, A., Alexander, B., Ault, A. P., Barth, M. C., Clegg, S. L., Collett Jr., J. L., Fahey, K. M., Hennigan, C. J., Herrmann, H., Kanakidou, M., Kelly, J. T., Ku, I.-T., McNeill, V. F., Riemer, N., Schaefer, T., Shi, G., Tilgner, A., Walker, J. T., Wang, T., Weber, R., Xing, J., Zaveri, R. A., and Zuend, A.: The acidity of atmospheric particles and clouds, Atmos. Chem. Phys., 20, 4809–4888, https://doi.org/10.5194/acp-20-4809-2020, 2020.

Riva, M., Chen, Y., Zhang, Y., Lei, Z., Olson, N. E., Boyer, H. C., Narayan, S., Yee, L. D., Green, H. S., Cui, T., Zhang, Z., Baumann, K., Fort, M., Edgerton, E., Budisulistiorini, S. H., Rose, C. A., Ribeiro, I. O., Oliveira, R. L., Santos, E. O., Machado, C. M. D., Szopa, S., Zhao, Y., Alves, E. G., Sá, S. S., Hu, W., Knipping, E. M., Shaw, S. L., Junior, S. D., Souza, R. A. F., Palm, B. B., Jimenez, J-L., Glasius, M., Goldstein, A. H., Pye, H. O. T., Gold, A., Turpin, B. J., Vizuete, W., Martin, S. T., Thornton, J. A., Dutcher, C. S., Ault, A. P., and Surratt, J. D.: Increasing isoprene epoxydiol-to-inorganic sulfate aerosol ratio results in extensive conversion of inorganic sulfate to organosulfur forms: Implications for aerosol physicochemical properties, Environ. Sci. Technol., 53, 8682–8694, https://doi.org/10.1021/acs.est.9b01019, 2019.

Schindelka, J., Iinuma, Y., Hoffmann, D., and Herrmann, H.: Sulfate radical-initiated formation of isoprene-derived organosulfates in atmospheric aerosols, Faraday Discuss., 165, 237–259, https://doi.org/10.1039/C3FD00042G, 2013.

Schuler, R. H., and Albarran, G.: The rate constants for reaction of radical •OH radicals with benzene and toluene, Radiat. Phys. Chem., 64, 189–195, https://doi.org/10.1016/S0969-806X(01)00497-2, 2002.

Shang, J., Passananti, M., Dupart, Y., Ciuraru, R., Tinel, L., Rossignol, S., Perrier, S., Zhu, T., and George, C.: SO_2 uptake on oleic acid: A new formation pathway of organosulfur compounds in the atmosphere, Environ. Sci. Technol. Lett., 3, 67–72, https://doi.org/10.1021/acs.estlett.6b00006, 2016.

Shrivastava, M., Cappa, C. D., Fan, J., Goldstein, A. H., Guenther, A. B., Jimenez, J. L., Kuang, C., Laskin, A., Martin, S. T.,

Ng, N. L., Petaja, T., Pierce, J. R., Rasch, P. J., Roldin, P., Seinfeld, J. H., Shilling, J., Smith, J. N., Thornton, J. A., Volkamer, R., Wang, J., Worsnop, D. R., Zaveri, R. A., Zelenyuk, A., and Zhang, Q.: Recent advances in understanding secondary organic aerosol: Implications for global climate forcing, Rev. Geophys., 55, 509–559, https://doi.org/10.1002/2016RG000540, 2017.

Singla, R., Ashokkumar, M., and Grieser, F.: The mechanism of the sonochemical degradation of benzoic acid in aqueous solutions, Res. Chem. Intermed., 30, 723–733, https://doi.org/10.1163/1568567041856963, 2004.

Smith, J. D., Kinney, H., and Anastasio, C.: Aqueous benzene-diols react with an organic triplet excited state and hydroxyl radical to form secondary organic aerosol, Phys. Chem. Chem. Phys., 17, 10227–10237, https://doi.org/10.1039/C4CP06095D, 2015.

Surratt, J. D., Gómez-González, Y., Chan, A. W. H., Vermeylen, R., Shahgholi, M., Kleindienst, T. E., Edney, E. O., Offenberg, J. H., Lewandowski, M., Jaoui, M., Maenhaut, W., Claeys, M., Flagan, R. C., and Seinfeld, J. H.: Organosulfate formation in biogenic secondary organic aerosol, J. Phys. Chem. A, 112, 8345–8378, https://doi.org/10.1021/jp802310p, 2008.

Surratt, J. D., Chan, A. W. H., Eddingsaas, N.C., and Seinfeld, J. H.: Reactive intermediates revealed in secondary organic aerosol formation from isoprene, Proc. Natl. Acad. Sci. U.S.A., 107, 6640–6645, https://doi.org/10.1073/pnas.0911114107, 2010.

Tang, S., Li, F., Tsona, N. T., Lu, C., Wang, X., and Du, L.: Aqueous-phase photooxidation of vanillic acid: A potential source of Humic-Like Substances (HULIS), ACS Earth Space Chem., 4, 862–872, https://doi.org/10.1021/acsearthspacechem.0c00070, 2020.

Thomas, A. E., Glicker, H. S., Guenther, A. B., Seco, R., Vega Bustillos, O., Tota, J., Souza, R. A. F., and Smith, J. N.: Seasonal investigation of ultrafine-particle organic composition in an eastern Amazonian rainforest, Atmos. Chem. Phys., 25, 959–977, https://doi.org/10.5194/acp-25-959-2025, 2025.

Tolocka, M. P., and Turpin, B.: Contribution of organosulfur compounds to organic aerosol mass, Environ. Sci. Technol., 46, 7978–7983, https://doi.org/10.1021/es300651v, 2012.

Tsona T. N., Lv, X., Tasheh, S. N., Ghogomu, J. N., and Du, L.: Atmospheric fate of organosulfates through gas-phase and aqueous-phase reactions with hydroxyl radicals: implications for inorganic sulfate formation, Atmos. Chem. Phys., 25, 8575–8590, https://doi.org/10.5194/acp-25-8575-2025, 2025.

Wang, L., Wu, R., and Xu, C.: Atmospheric oxidation mechanism of benzene. fates of alkoxy radical intermediates and revised mechanism, J. Phys. Chem. A, 117, 14163–14168, https://doi.org/10.1021/jp4101762, 2013.

Wang, S., Zhou, S., Tao, Y., Tsui, W. G., Ye, J., Yu, J. Z., Murphy, J. G., McNeill, V. F., Abbat, J. P. D., and Chan, A. W. H.: Organic peroxides and sulfur dioxide in aerosol: source of particulate sulfate, Environ. Sci. Technol., 53, 10695–10704, https://doi.org/10.1021/acs.est.9b02591, 2019.

Wang, Y., Hu, M., Guo, S., Wang, Y., Zheng, J., Yang, Y., Zhu, W., Tang, R., Li, X., Liu, Y., Le Breton, M., Du, Z., Shang, D., Wu, Y., Wu, Z., Song, Y., Lou, S., Hallquist, M., and Yu, J.: The secondary formation of organosulfates under interactions between biogenic emissions and anthropogenic pollutants in summer in Beijing, Atmos. Chem. Phys., 18, 10693–10713,

https://doi.org/10.5194/acp-18-10693-2018, 2018.

Wang, Y., Zhao, Y., Wang, Y., Yu, J.-Z., Shao, J., Liu, P., Zhu, W., Cheng, Z., Li, Z., Yan, N., and Xiao, H.: Organosulfates in atmospheric aerosols in Shanghai, China: seasonal and interannual variability, origin, and formation mechanisms, Atmos. Chem. Phys., 21, 2959–2980, https://doi.org/10.5194/acp-21-2959-2021, 2021.

Wang, Y., Ma, Y., Kuang, B., Lin, P., Liang, Y., Huang, C., and Yu, J. Z.: Abundance of organosulfates derived from biogenic volatile organic compounds: Seasonal and spatial contrasts at four sites in China, Sci. Total Environ., 806, 151275, https://doi.org/10.1016/j.scitotenv.2021.151275, 2022.

Xu, R., Ge, Y., Kwong, K. C., Poon, H. Y., Wilson, K. R., Yu, J. Z., and Chan, M. N.: Inorganic sulfur species formed upon heterogeneous •OH oxidation of organosulfates: A case study of methyl sulfate, ACS Earth Space Chem., 4, 2041–2049, https://doi.org/10.1021/acsearthspacechem.0c00209, 2020.

Xu, R., Ng, S. I. M., Chow, W. S., Wong, Y. K., Wang, Y., Lai, D., Yao, Z., So, P.-K., Yu, J. Z., and Chan, M. N.: Chemical transformation of α-pinene-derived organosulfate via heterogeneous OH oxidation: implications for sources and environmental fates of atmospheric organosulfates, Atmos. Chem. Phys., 22, 5685–5700, https://doi.org/10.5194/acp-22-5685-2022, 2022.

Xu, R., Chen, Y., Ng, S. I. M., Zhang, Z, Gold, A., Turpin, B. J., Ault, A. P., Surratt, J.D., and Chan, M. N.: Formation of inorganic sulfate and volatile nonsulfated products from heterogeneous hydroxyl radical oxidation of 2-methyltetrol sulfate aerosols: Mechanisms and atmospheric implications, Environ. Sci. Technol. Lett., 11, 968–974, https://doi.org/10.1021/acs.estlett.4c00451, 2024.

Yang, T., Xu, Y., Ye, Q., Ma, Y.-J., Wang, Y.-C., Yu, J.-Z., Duan, Y.-S., Li, C.-X., Xiao, H.-W., Li, Z.-Y., Zhao, Y., and Xiao, H.-Y.: Spatial and diurnal variations of aerosol organosulfates in summertime Shanghai, China: potential influence of photochemical processes and anthropogenic sulfate pollution, Atmos. Chem. Phys., 23, 13433–13450, https://doi.org/10.5194/acp-23-13433-2023, 2023.

Yao, M., Zhao, Y., Hu, M., Huang, D., Wang, Y., Yu, J. Z., and Yan, N.: Multiphase reactions between secondary organic aerosol and sulfur dioxide: kinetics and contributions to sulfate formation and aerosol aging, Environ. Sci. Technol. Lett., 6, 768–774, https://doi.org/10.1021/acs.estlett.9b00657, 2019.

Yao, M., Zhao, Y., Chang, C., Wang, S., Li, Z., Li, C., Chan, A. W. H., and Xiao, H.: Multiphase reactions between organic peroxides and sulfur dioxide in internally mixed inorganic and organic particles: key roles of particle phase separation and acidity, Environ. Sci. Technol., 57, 15558–15570, https://doi.org/10.1021/acs.est.3c04975, 2023.

Zhang, H., Worton, D. R., Lewandowski, M., Ortega, J., Rubitschun, C. L., Park, J-H., Kristensen, K., Campuzano-Jost, P., Day, D. A., Jimenez, J. L., Jaoui, M., Offenberg, J. H., Kleindienst, T. E., Gilman, J., Kuster, W. C., Gouw, J., Park, C., Schade, G. W., Frossard, A. A., Russell, L., Kaser, L., Jud, W., Hansel, A., Cappellin. L., Karl, T., Glasius, M., Guenther, A., Goldstein, A. H., Seinfeld, J. H., Gold, A., Kamens, R. M., and Surratt, J. D.: Organosulfates as tracers for secondary organic aerosol (SOA) formation from 2-Methyl-3-Buten-2-ol (MBO) in the atmosphere, Environ. Sci. Technol., 46, 9437–9446, https://doi.org/10.1021/es301648z, 2012.